Journal of Alloys and Compounds 1024 (2025) 180272

Contents lists available at ScienceDirect

Journal of Alloys and Compounds

journal homepage: www.elsevier.com/locate/jalcom

Synthesis of ternary and quaternary MAX phases in Ti/Cr/Nb/V-Al-C system by high energy ball milling and pressureless spark plasma sintering

Grzegorz Kubicki [a,b,*], Jakub Wiśniewski [a,b], Sophia Alexandra Tsipas [c], Albert Kania [a], Adam Patalas [d], Jarosław Jakubowicz [e], Dariusz Garbiec [a]

[a] Łukasiewicz Research Network – Poznań Institute of Technology, 6 Ewarysta Estkowskiego St., Poznan 61-755, Poland
[b] Faculty of Materials Engineering and Technical Physics, Poznan University of Technology, 24 Jana Pawla II St., Poznan 61-138, Poland
[c] Departamento de Ciencia e Ingeniería de Materiales e Ingeniería Química, IAAB, Universidad Carlos III de Madrid, Avda. de la Universidad, 30, 28911 Leganés, Madrid, Spain
[d] Institute of Mechanical Technology, Poznan University of Technology, ul. Piotrowo 3, Poznań 60-965, Poland
[e] Institute of Materials Science and Engineering, Poznan University of Technology, 24 Jana Pawla II St., Poznan 61-138, Poland

ARTICLE INFO

Keywords:
Spark Plasma Sintering
High-energy ball milling
MAX phase
Indentation
Structural analysis
Thermogravimetry

ABSTRACT

The search for MAX phase synthesis methods that allow good energy efficiency and phase purity remains ongoing. In this work, high energy ball milling and pressureless spark plasma sintering were used to synthesize ternary and quaternary MAX phases from Ti/Nb/V/Cr-Al-C system in a powder form. The powders were densified in a separate spark plasma sintering process. Synthesized powders and bulks structure were studied using scanning electron microscope and X-ray diffraction. Chemical composition was determined using energy dispersive X-ray spectroscopy and carbon and oxygen analyzers. Thermal oxidation and mechanical properties were assessed using thermogravimetry and nanoindentation. The high energy ball milling and pressureless spark plasma sintering route allowed fabrication of both ternary and quaternary MAX phase systems, except TiCrAlC and NbCrAlC. The synthesized MAX phases purity was in the range of 92–98 %, according to Rietveld refinement. Secondary phases consisted of M-X carbides and M-A intermetallics, as well as aluminum oxide. The highest hardness and elastic modulus values were observed for Nb_2AlC and NbVAlC MAX phases. Thermogravimetric tests showed limited oxidation rate of MAX phases within 20–900°C range, except for Ti_2AlC, which could be attributed to increased oxygen content before test. This work presents a beneficial method for fabrication of relatively phase-pure MAX phases using different M-type elements as precursor materials.

1. Introduction

MAX phases are a ternary carbide and nitride group with a general formula $M_{n+1}AX_n$, where the M stands for early transition metal, A – group 13 or 14 element and X, carbon or nitrogen. These materials were first discovered in 1960s by Rohde et al. [1] as Ti-S-C and Zr-S-C compounds, and later by Nowotny et al. [2], who described them as ternary carbide group with [3] a hexagonal, layered structure and a P_{63}/mmc symmetry. In 1996, Barsoum et al. [4] obtained dense bulks of Ti_3SiC_2 and described its unique set of properties characteristic to both the metallic and ceramic materials group. Since then, MAX phases have gained increasing attention. In 2011 [5], the research team from Drexel University discovered that by selectively etching the A element out of MAX phase, graphene-like MXenes with similar (and in some cases superior) functional properties can be obtained. Since then, MAX phases have gained more interest as a MXene precursor [6], instead of construction applications such as high temperature, corrosion or radiation resistant material [7,8]. The distinctive properties set of MAX phases warrant several possible demanding applications, such as nuclear fuel cladding [3], bond coat for thermal barrier systems [9], high-temperature camouflage systems [10] and many more [11], which have been studied using ternary MAX phase variants. Currently, much interest is focused on MAX phases containing several M-type elements, especially in combination with in-silico modelling approaches, such as density functional theory (DFT), that can used predict the structure stability [12] and properties [13] of MAX phases and other novel structures [14]. The results of both theoretical and experimental works indicate that medium [15] and high-entropy [16] MAX phases have

* Corresponding author at: Łukasiewicz Research Network – Poznań Institute of Technology, 6 Ewarysta Estkowskiego St., Poznan 61-755, Poland.
E-mail address: grzegorz.kubicki@pit.lukasiewicz.gov.pl (G. Kubicki).

https://doi.org/10.1016/j.jallcom.2025.180272
Received 14 March 2025; Received in revised form 3 April 2025; Accepted 6 April 2025
Available online 7 April 2025

superior microwave absorption capabilities, increased mechanical strength [17] and thermal insulation performance [18]. Moreover, their MXene counterparts exhibit high-efficiency electromagnetic wave absorption capabilities [19] and can be used in several energy storage applications, such as lithium-ion, lithium-sulfur battery as well as supercapacitor components [20].

MAX phases have been obtained using various approaches, the most common being solid-state reaction during annealing or sintering of elementary or carbide precursors. This process may be conducted using various heating techniques: pressureless sintering (PS) [21,22], hot pressing (HP) [23], field-assisted sintering /spark plasma sintering (FAST/SPS), molten salt-shielded synthesis (MS^3) [24,25] and many others. Various other approaches have also been proposed, such as arc melting of the precursor materials [26], annealing of amorphous magnetron sputtered films [27,28], or combustion synthesis enabled by aluminothermic reduction of M element oxide precursor [29–31]. The FAST/SPS technique has been proven to produce the MAX phases of high phase purity and allow to conduct the synthesis as well as densification in one process [32,33]. This method also provides other advantages, such as short heating time and lower synthesis temperature, resulting in improvement of productivity. The FAST/SPS main disadvantage is limited scalability due to high infrastructure costs and technical capability for large-scale production. Direct synthesis from elementary precursors is also limited, as the self-heating synthesis (SHS) reaction takes place during heating of the material, leading to intense thermal gradients, evaporation of A-element (most commonly aluminum) and thermal degradation of the already synthesized MAX phase. While most of the FAST/SPS and other sintering techniques focus on creating dense bulk MAX phases, pressureless variants of the process [34,35] may also be applied to keep the resulting material in scaffold or powder form [36, 37]. In this way, it is easier to create powder feedstocks for MXene synthesis [38,39], thermal spraying [40–42], and other technologies. To improve the scalability of the FAST/SPS technique, high energy ball milling (HEBM) may be used [43] to pre-alloy the precursor powders and trigger the SHS reaction before the sintering stage [44], greatly improving the repeatability and scalability of the synthesis, regardless of the sintering tools size thanks to more even temperature distribution throughout the synthesis.

This work aims to fulfill three main objectives. Firstly, to study the feasibility of high energy ball milling-pressureless spark plasma sintering (HEBM-PSPS) route for synthesis of various ternary and quaternary MAX phases, to synthesize medium and high-entropy MAX phases in the future using the same methodology. Secondly, to develop the densification parameters via FAST/SPS of synthesized MAX phases. The last objective is to provide thorough structural, thermal, and mechanical properties data of synthesized and densified MAX phase bulks and powders.

To fulfill these objectives, the authors have conducted HEBM-PSPS synthesis trials from Ti/Cr/Nb/V-Al-C ternary and quaternary mixtures and densified the synthesized powder in a two-stage process. At each stage, structural assessment was conducted using X-ray diffraction (XRD), scanning electron microscopy (SEM) and oxygen and carbon analysis. Moreover, the oxidation resistance of the powders were determined by thermogravimetry (TG), additionally, the mechanical properties of the densified materials were examined by Vickers hardness measurements and nanoindentation tests.

2. Materials and methods

Elementary powders of: titanium (325 mesh, 99.5 %, AEM Deposition, Hunan, China), niobium (325 mesh, >99.8 %, Thermo Fisher Scientific, Waltham, Massachusetts, United States), chromium (325 mesh, 99.5 %, KAMB Import Export, Warsaw, Poland), vanadium (200 mesh, >99.5 %, ChemPUR, Karlsruhe, Germany), aluminum (100 mesh, 98.5 %, ChemPUR, Karlsruhe, Germany) and graphite (7–11 μm, >99 %, Thermo Fisher Scientific, Waltham, Massachusetts, United States) were used as starting powders for the MAX phase synthesis trials. The powders were mixed in a 2:1.1:0.9 stoichiometry for ternary MAX phases and 1:1:1.1:0.9 for quaternary MAX (further referred to as MMAX) phases and high energy ball milled using Pulverisette 5 Classic Line (Fritsch GmbH, Weimar, Germany) planetary ball mill using tungsten carbide milling jars with a capacity of 250 ml for 12 h at 300 rpm. The ball-to-powder ratio (BPR) was kept at 10:1, while the diameter of tungsten carbide balls was 10 mm. This approach was used for Ti-Al-C, Nb-Al-C, V-Al-C, Cr-Al-C, Ti-Nb-Al-C, Ti-V-Al-C, Ti-Cr-Al-C, Nb-V-Al-C, Nb-Cr-Al-C, Cr-V-Al-C systems.

After milling, the powders were inserted into a graphite die with an inner diameter of 40 mm, and a height of 60 mm. Using Papyex N998 graphite foil (Mersen, Gennevilliers, France) with a thickness of 0.4 mm and a graphite tools (2334 graphite grade, Mersen, Gennevilliers, France), tool setup was assembled to perform PSPS process using the HP D 25/3 furnace (FCT Systeme GmbH, Frankenblick, Germany) under sintering parameters shown in Table 1. All operations on powders preceding synthesis of MAX phases were carried out in an inert atmosphere of argon in a LABstar Pro (MBRAUN, Stratham, New Hampshire, USA) glovebox to prevent oxidation of starting and as-milled powders.

The resulting sintered scaffolds were grounded into powder using agate mortar and put again into graphite tools for densification trails. Samples with a diameter of 25.4 mm and a height of 5 mm were sintered using parameters shown in Table 2 and, after sandblasting, wet grinding with a SiC paper was carried out to prepare flat surface for XRD examination, and subsequently the materials were cut into smaller pieces for further tests.

Density measurements were taken based on Archimedes' principle using an Explorer EX225DM scale (OHAUS, Nänikon, Switzerland). X-ray diffraction measurements were made using the Aeris Research diffractometer (Malvern PANalytical, Malvern Worcestershire, United Kingdom). The diffraction was conducted with 5–75° 2θ diffraction angle range using copper Kα (λ=1.54 Å) radiation. The diffraction data was obtained from PDF 5 + 2024 (International Centre for Diffraction Data, New-town Square, Pennsylvania, USA) database. Rietveld refinement method [45] via Highscore Plus ver. 5.1a software was used for lattice parameters, microstrain and crystal size determination.

The scanning electron micrographs of powders morphology and bulks microstructure were obtained using Teneo LoVac (FEI Company, Hillsboro, Oregon, United States) high resolution scanning electron microscope. The oxygen content in the synthesized material was determined using TC500 (LECO Corporation, St. Joseph, Michigan, United States) oxygen-nitrogen analyzer. The powder material was weighted and placed inside tin foil and nickel gasket, then inductively heated up inside a graphite crucible with 0.5 g of graphite powder addition. The carbon content was determined using CS-200 (LECO Corporation, St. Joseph, Michigan, United States) carbon-sulfur analyzer. The powders were put inside the alumina crucible alongside combustion accelerator and burned down in oxygen atmosphere. Both oxygen and carbon content were determined using the infrared emission of carbon dioxide emitted during the burning of material. The contents of M, A and X elements were recalculated using EDS results for M and A and carbon analyzer results for X content (Eq. 1).

$$\begin{aligned} \%\text{wt M} &= (100\% - \%\text{wt.C[Leco]}) \quad \frac{\%\text{wt.M[EDS]}}{\%\text{wt.M} + \text{A[EDS]}} \%\text{wt A} \\ &= (100\% - \%\text{wt.C[Leco]}) \quad \frac{\%\text{wt.A[EDS]}}{\%\text{wt.M} + \text{A[EDS]}} \end{aligned} \tag{1}$$

Table 1
MAX phase synthesis via pressureless spark plasma sintering process parameters.

Sintering temperature	Compaction pressure	Holding time	Heating rate	Atmosphere
1100 °C	none	5 min	100 °C/min	Vacuum (0.05 mbar)

Table 2
Densification via Spark Plasma Sintering (SPS) process parameters.

Sintering temperature	Compaction pressure	Holding time	Heating rate	Atmosphere
1200–1300 °C	30 MPa	5 min	100 °C/min	Vacuum (0.05 mbar)

Eq. 1.Recalculation formula for M- and A-element content.

Thermogravimetric analysis was made using simultaneous thermal analyzer 6000 (PerkinElmer, Waltham, Massachusetts, United States) in 35–900 °C range, with heating rate of 10 °C/min with synthetic air flow of 20 ml/min. The powders (60–120 mg) were mortar-grounded and placed within the crucible prior to analysis. The Vickers hardness tests were conducted using Wolpert UH930 (Buehler, Lake Bluff, Illionois, United States) universal hardness tester at 30 kgf load for 15 s, according to ISO 6507–1 standard. The nanoindentation tests were conducted using Picodentor HM500 (Fischer Technology Inc., Windsor, CT, USA) indenter with following parameters: a maximum load of 30 mN for MAX phase area examination and 300 mN for multi-grain loaded during 20 s and dwell time of 5 s. The elastic modulus and hardness determination was based on Olivier and Pharr technique [46,47].

3. Results & discussion

3.1. Analysis of HEBM – PSPS synthesis and SPS densification

The milling resulted in MAX phase formation in following cases: Ti-Al-C, Nb-Al-C, Ti-Nb-Al-C, Ti-V-Al-C (Table 3). The main reason is exothermic SHS reaction between titanium (or niobium) and carbon [48]. The reaction provides the necessary temperature for reaction with aluminum, partially forming MAX phase during the milling stage, as described in other works concerning MAX phase synthesis [44,49]. While titanium and niobium was present in Ti-Cr-Al-C and Nb-Cr-Al-C, the self-heating reaction did not form MAX phase, due to limited solubility [50,51] of these systems. Instead, a structure consisting of MX carbide, M-A and M-M intermetallic phases was obtained. In the case of Cr-Al-C, V-Al-C, Cr-V-Al-C and Nb-V-Al-C mixtures the milling did not result in formation of significant amount of MAX phase, implicating that the formation of carbides from these mixtures was less exothermic than titanium- and niobium-based ones. Nevertheless, the absence of self-heating reaction did not hinder the MAX phase formation during the PSPS process.

While the SHS reaction allows the formation of MAX phase during the milling phase, yet at most of the cases it led to formation of a MAX, intermetallic and carbide phases (Table 3). High-temperature annealing or sintering step is required (PSPS) to let the remaining carbide and intermetallic phases to react [52], forming a MAX phase. The detailed diffractograms of synthesized powders as well as bulks have been placed in supplementary information (Figures S1–S5).

The densification by FAST/SPS at higher temperature (1200 °C) than the pressureless synthesis allowed to increase the MAX phase content even further (Figures S1–S5), signifying that the synthesis temperature may need to be increased according to thermal properties of specific M-elements. The determined purities of the final sintered MAX phase bulks ranged from 92 % to 98 % according to Rietveld refinement results (Table 4). The lowest purity was observed for Ti_2AlC. In this case, significant presence of aluminum oxide phase was detected, signifying possible oxygen contamination. The possible source of contamination was during milling phase, during exothermic formation of titanium carbide the temperature and pressure within the milling tools are greatly increased, which slightly unseals the milling tools, enabling mixing of the argon atmosphere with air. In order to increase the purity of the synthesized MAX phases, several steps may be taken: optimization of precursor stoichiometries (to reduce the carbide/intermetallic phase content), usage of more pure precursor material and improvement of milling tools seal strength (limitation of oxide impurity).

The FAST/SPS sintering temperature of 1200 °C resulted in densification (open porosity below 2 %) of most of the materials (Table 5), except Nb_2AlC and NbVAlC. To produce more densified bulks, an increase of sintering temperature by 100 °C for Nb_2AlC and NbVAlC was tested. While the increase of the process temperature led to reduction of open porosity below 2 % for NbVAlC, it was not sufficient to sufficiently densify Nb_2AlC. Further optimization of the sintering parameters (temperature, dwell time, pressure) will be made in the future works.

The Rietveld refinement results (Table 6) show that the obtained MAX phase bulks have crystallite size within 0.5–2 μm range. The increased densification temperature for Nb_2AlC and NbVAlC resulted only in slight difference in the resulting crystal size. While most of the samples had relatively small microstrain, The Cr_2AlC and CrVAlC exhibited higher values. This may be attributed to their larger coefficient of thermal expansion (CTE) [53], in comparison to other MAX phases [54], resulting in increased expansion and shrinkage during sintering cycle, leading to increased strain generation form thermal gradients. Due to limited data availability, it is yet to be proven if the same mechanism could apply to NbVAlC, in which case the microstrain values were even higher than in the case of Cr_2AlC and CrVAlC.

Table 3
Phase composition of milled/synthesized/densified MAX phases.

	MAX phase type	Identified phases		
		Milled material (12 h)	Pressureless synthesized scaffold	Densified bulk
1	Ti_2AlC	Ti_2AlC, TiC, Ti_3Al	Ti_2AlC, Ti_3AlC_2, $TiAl_3$, Al_2O_3	Ti_2AlC, Ti_3AlC_2, $TiAl_3$, Al_2O_3
2	Cr_2AlC	Cr, Cr_5Al_8, CrC	Cr_2AlC, Cr_2Al	Cr_2AlC, Cr_2Al, $Cr_{23}C_6$
3	Nb_2AlC	Nb_2AlC, NbC, NbAl	Nb_2AlC, Nb_3Al_2C,	Nb_2AlC, Nb_2C, NbAl
4	V_2AlC	V, Al, V_4AlC_3	V_2AlC, V_4AlC_3, V_4Al_{23}	V_2AlC, V_4AlC_3
5	TiNbAlC	TiNbAlC, NbC, Ti_3Al	TiNbAlC, VAl	TiNbAlC, $TiAl_3$
6	TiCrAlC	Ti, Cr, TiC, $TiCr_2$, Ti_3Al	TiC, $TiCr_2$, Cr_2Al, Cr_5Al_8	TiC, Cr_2Al, Cr_5Al_8
7	TiVAlC	TiVAlC, TiVC, Ti_3Al	TiVAlC, VAl	TiVAlC, V_2C
8	CrVAlC	Cr, V, Al, V_4C_3, V_2C	CrVAlC, Cr_2Al, Cr_2C	CrVAlC, Cr_2Al, Cr_2C
9	NbVAlC	Nb, NbC, V_3Al, Nb_3Al_2C	NbVAlC, NbC, VC, $NbAl_3$, V_3Al	NbVAlC, $NbAl_3$, V_3Al
10	NbCrAlC	Cr_3Al, NbC, Nb_2Al;	NbC, Cr_2Al	NbC, Cr_2Al, Cr_2AlC

3.2. Microstructure and chemical composition assessment

All materials obtained during this study were divided into three groups. The first group of ternary MAX phases: Cr_2AlC, Nb_2AlC, Ti_2AlC and V_2AlC, the second group of synthesized quaternary MAX phases

Table 4
Quantitative phase composition of sintered bulks according to Rietveld refinement.

Material	Quantitative phase composition
Ti_2AlC	**Ti_2AlC – 92.9 %,** Ti_3AlC_2 – 4.5 %, Al_2O_3 – 2.5 %
Cr_2AlC	**Cr_2AlC – 97.9 %,** Cr_2Al – 1.3 %, $Cr_{23}C_6$ – 0.8 %
Nb_2AlC (1300 °C)	**Nb_2AlC – 98.7 %,** Nb_2C – 0.7 %, NbC – 0.6 %
V_2AlC	**V_2AlC – 100 %**
TiNbAlC	**TiNbAlC – 99.2 %,** $TiAl_3$ – 0.8 %
TiCrAlC	TiC – 59.3 %, Cr_2Al – 8.3 %, Cr_5Al_8 – 32.4 %
TiVAlC	**TiVAlC – 98.9 %,** V_2C – 1.1 %
CrVAlC	**CrVAlC – 99.0 %,** Cr_2Al – 0.5 %, Cr_2C – 0.5 %
NbVAlC (1300 °C)	**NbVAlC – 96.6 %,** $NbAl_3$ – 3.4 %
NbCrAlC	NbC – 71.0 %, Cr_2Al – 16.8 %, Cr_2AlC – 12.2 %

Table 5
Densification temperature optimization.

Material	Sintering temperature [°C]	Bulk density [g/cm^3]	Open porosity [%]	Apparent solid density [g/cm^3]	Theoretical density (PDF5 +) [g/cm^3]
Ti_2AlC	1200	**4.05**	0.5	4.07	4.04
Cr_2AlC	1200	**5.12**	0.8	5.16	5.23
V_2AlC	1200	**4.87**	1.8	4.95	4.85
Nb_2AlC	1200	**5.9**	6.7	6.33	6.37
Nb_2AlC	1300	**5.93**	3.9	6.17	6.37
TiNbAlC	1200	**5.22**	0.5	5.25	5.28
TiCrAlC	1200	**4.69**	1.3	4.75	-
TiVAlC	1200	**4.39**	0.8	4.43	4.46
CrVAlC	1200	**5.01**	0.3	5.02	5.01
NbVAlC	1200	**4.95**	9.9	5.49	5.6
NbVAlC	1300	**5.51**	0.7	5.56	5.6
NbCrAlC	1200	**6.02**	1.1	6.09	-

Measurement errors calculated for bulk density and open porosity did not exceed values of 0.001 g/cm^3 and 0.01 %, respectively.

Table 6
Rietveld refinement analysis result of SPS-densified MAX phase bulks.

Material	Lattice parameter [Å]			Microstrain [%]		Crystallite size [Å]	
	Value		Error				
	a/b	c		Value	Error	Value	Error
Nb2AlC	3.107	13.870	0.002	0.020	0.002	1422.6	32.2
Nb_2AlC (1300 °C)	3.106	13.867	0.001	0.020	0.001	1797.3	50.7
Ti_2AlC	3.059	13.657	0.003	0.021	0.003	1497.4	40.2
Cr_2AlC	2.860	12.818	0.007	0.102	0.004	813.2	29.4
V_2AlC	2.915	13.129	0.004	0.055	0.003	1399.0	67.0
NbVAlC	3.020	13.532	0.009	0.218	0.003	631.6	14.8
NbVAlC (1300°C)	3.024	13.541	0.008	0.224	0.002	572.5	7.8
TiNbAlC	3.077	13.790	0.002	0.023	0.002	1821.6	69.6
CrVAlC	2.893	12.984	0.008	0.155	0.003	722.2	19.8
TiVAlC	2.982	13.427	0.004	0.048	0.003	1036.2	30.7

(referred as MMAX), which includes CrVAlC, NbVAlC, TiNbAlC and TiVAlC. Two of the studied materials (NbCrAlC and TiCrAlC) did not form MMAX phase at any processing step. Nevertheless, to maintain the clarity of the reported results, both of them will be subsequently described according to their chemical composition as "NbCrAlC" and "TiCrAlC". As illustrated in Fig. 1, microstructure examination and EDS analysis (Figures S11–S18) of cross-sections of ternary MAX reveals the presence of a dominant MAX phase (blue arrows), with Al_2O_3 precipitations (red arrows) identified as the primary impurity. This oxide is a common impurity of Al-consisting MAX phases [55]. It is possible that both aluminum and transition metal powders could be a potential source of oxygen, due to their high potential for oxygen absorption and possible exposure to air during material transport. It is also possible that the oxygen might have been introduced during the milling stage through small leaks in the milling jar sealing. In certain instances (e.g., Ti_2AlC), the presence of MA intermetallic phases (in this case, Ti_3Al) can be discerned in the microstructure (orange arrows), possibly attributable to local carbon deficiency. Conversely, local carbon excess can result in the formation of MX carbide phases (violet arrows), as evidenced by the $Cr_{23}C_6$ phase in the Cr_2AlC material. Although the densification process resulted in relatively dense bulks, some residual porosity (green arrows) is also present in the microstructure of the materials. It is noteworthy that, not all phases indicated in the XRD measurements were distinguishable on the SEM micrographs and some phases visible in the microstructure observations (e.g., Al_2O_3) were not indicated in XRD diffractograms (Figures S1–S5). This is connected to the resolution capacity of the examination methods and the range of data collection.

Considering the observations about the microstructure of cross-sections of MMAX materials (Fig. 2), analogous conclusions can be drawn to those of ternary MAX materials. In all cases, the dominant phase is the quaternary MAX phase. Moreover, Al_2O_3 particles were identified during microstructural analysis. Apart from the porosities marked with green arrows, other characteristic elements (such as intermetallic compounds or carbides) were not observed in the microstructure of the materials studied (Figures S15–S18).

Powder mixtures of Nb-Cr-Al-C and Ti-Cr-Al-C formed different intermetallic compounds and carbides at subsequent synthesis step, but no MMAX phase was formed at any of those steps. Final microstructure of the NbCrAlC material consisted of NbC, Cr_2Al and Cr_2AlC phases indicated in XRD measurements, and of Al_2O_3 oxide observed on SEM micrographs and EDS analysis (Fig. 3 and S19). Depending on stoichiometry of Cr-Al intermetallic two light- and dark-grey areas can be distinguished in the microstructure of the NbCrAlC material. The NbC carbide is distinguished by its regular and sharp shape, which is characteristic of cubic MC carbides. An analogous morphology is exhibited by the TiC in the TiCrAlC material. (Fig. 3). In both, Nb-Cr-Al-C and Ti-Cr-Al-C, Al_2O_3 oxide is present as more or less rounded-shape particles of < 1 μm size. Cr-Al intermetallic compounds present in the TiCrAlC material include Cr_5Al_8 phase (dark-grey area) and Cr_2Al (light-grey area). Noteworthy, light-grey phase is not homogenous and consists of lighter needle-like Cr-Al intermetallic with higher chromium content, as indicated by EDS analysis (Figures S19–S20) than surrounding Cr-Al intermetallic matrix. Considering the multiplicity of Cr-Al intermetallic compounds, it can be assumed that, apart from the presence of TiC and Al_2O_3, the microstructure of the TiCrAlC material can be formed by a mixture of compounds such as Cr_2Al, Cr_5Al_8, Cr_4Al_9, $CrAl_4$, Cr_2Al_{11} and $CrAl_7$, with Cr_2Al and Cr_5Al_8 dominating phases as evidenced by XRD measurements.

The EDS measurements of M-element and aluminum content were made of the areas, where no presence of aluminum oxide (black spots) or other impurities was visible, and the results are shown in Table 7. The EDS results did not indicate oxygen content (except for Cr_2AlC) collected from those areas (Figures S11-S20), which suggests, that the oxygen present in the MAX and MMAX structures was mainly in oxide form. To fully determine the possible substitution of carbon atoms by oxygen, other methods, like secondary-ion mass spectrometry [56] may be used in the future. By combining the EDS-derived M and A-element contents with carbon analysis results using Eq. 1, it is possible to estimate the synthesized MAX phase stoichiometry deviation. The obtained values (Table 7) indicate notable aluminum deficiency in all cases, but the MAX phase structure remained stable due to high tolerance of Al vacancies of MAX phases [57], as proven by X-Ray diffraction (Figures S1-S5) and characteristic lamellar regions visible in both powder (Figures S6-S10) and bulk microstructures (Figs. 1 and 2). This may indicate, that the aluminum loss, previously attributed to evaporation during synthesis [33], could also be attributed to reaction with oxygen adsorbed by the precursor particles, resulting in formation and growth of Al_2O_3 seeds [55] during HEBM-SPS synthesis, especially when the synthesis is being conducted at 1100 °C, reducing the evaporation rate of aluminum.

3.3. Mechanical properties of densified bulks

Table 8 presents the values gathered by hardness and indentation tests. The indentation curves comparison has been included in supplementary information (Figure S21). In general, the MMAX phases exhibited higher hardness and stiffness in comparison to their MAX counterparts. While the typical modulus values for MAX phases range from 250 to 350 GPa [58], the obtained values are lower due to the remaining porosity after SPS densification. The highest hardness and elastic modulus levels were observed for niobium-based MAX and MMAX phases (Nb_2AlC, TiNbAlC and NbVAlC). Both lower hardness and modulus of V_2AlC is the result of higher porosity (Table 5) as well as larger single pore size (Fig. 1, lower right) than in other sintered bulks.

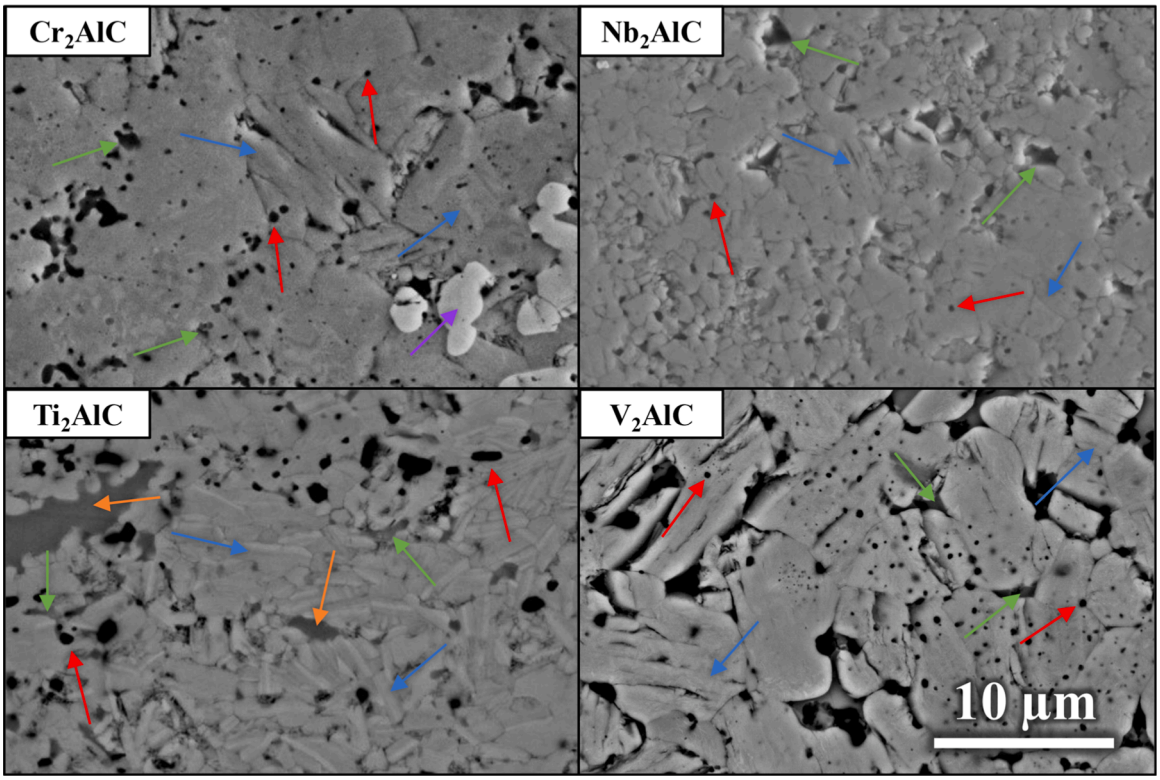

Fig. 1. Microstructure of the cross-sections of Cr_2AlC, Nb_2AlC, Ti_2AlC and V_2AlC: blue arrows – M_2AX phase, red arrows – Al_2O_3; orange arrows – MA intermetallics; violet arrows – MX carbides; green arrows – porosity.

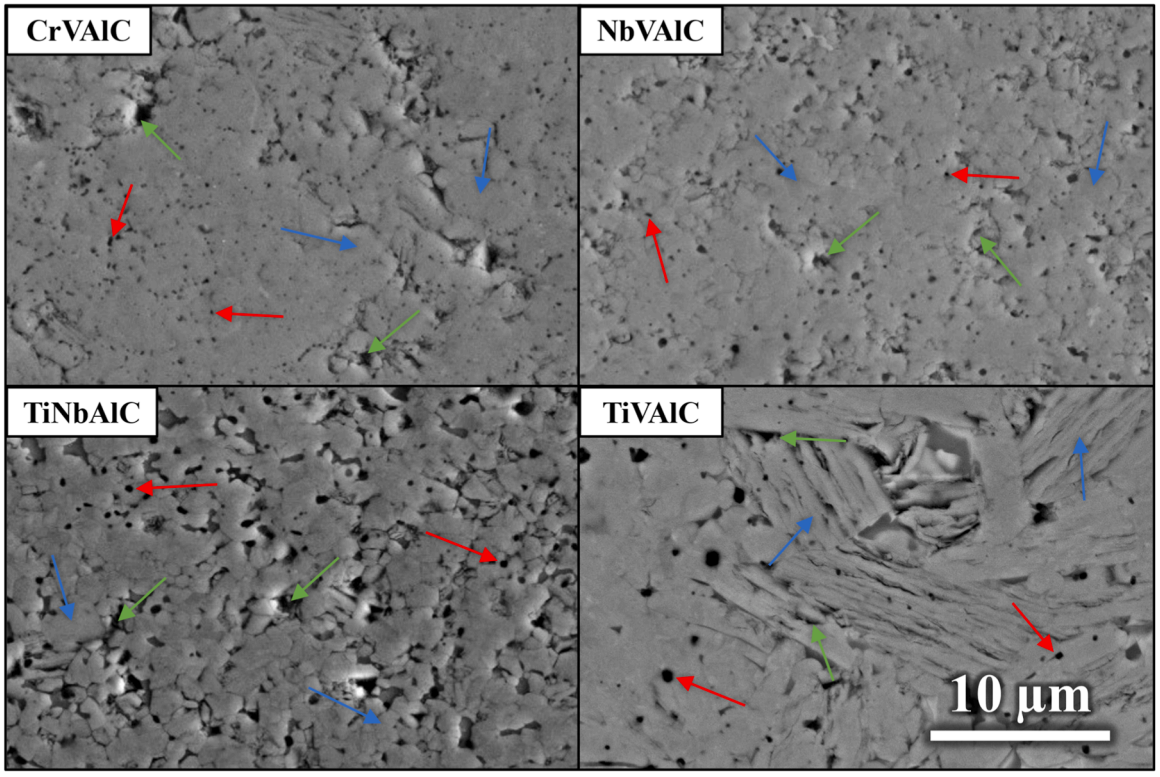

Fig. 2. Microstructure of the cross-sections of CrVAlC, NbVAlC, TiNbAlC and TiVAlC: blue arrows – MMAX phase, red arrows – Al_2O_3; green arrows – porosity.

No direct correlations between the oxygen content and mechanical properties of the synthesized MAX and MMAX phase were observed, however increased deviation of the results was observed for Ti_2AlC, due to the presence of large alumina grains within the microstructure (Fig. 1). It is noteworthy, lower values of hardness and modulus were observed for chromium- and vanadium containing compounds – these

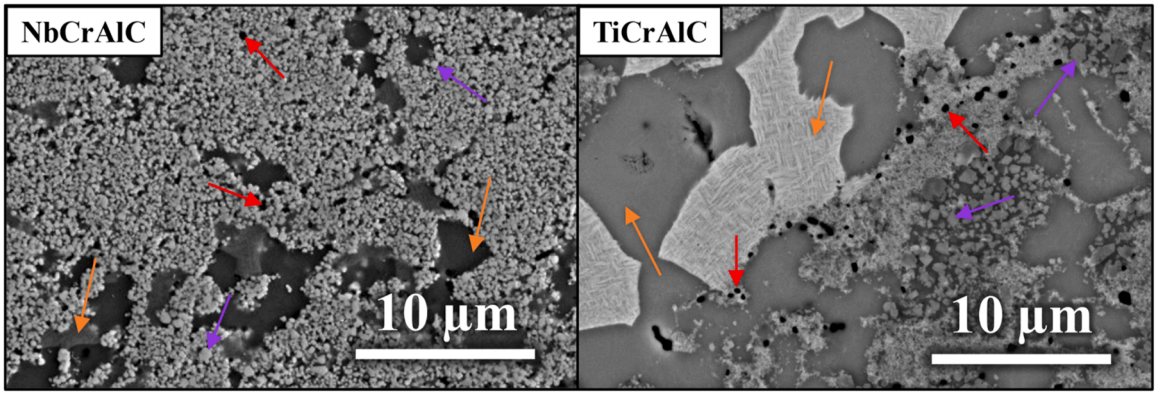

Fig. 3. Microstructure of the cross-sections of NbCrAlC and TiCrAlC: red arrows – Al_2O_3; orange arrows – MA intermetallics; violet arrows – MX carbides.

Table 7
M, A and X element contents determination of synthesized MAX phases.

Determined by:	SEM-EDS (MAX phase area)				Leco TC500	Leco CS200	
	M-Element [wt%]		Aluminum Content [wt%]		Oxygen content [wt%]	Carbon content [wt%]	
	Exp.	Theo.	Exp.	Theo.		Exp.	Theo.
Ti_2AlC	72.978 ± 4.853	71.058	16.659 ± 1.107	20.027	2.100 ± 0.014	9.357 ± 0.043	8.915
Cr_2AlC	74.192 ± 4.600	72.730	16.561 ± 1.027	18.870	0.895 ± 0.165	7.687 ± 0.727	8.400
V_2AlC	73.948 ± 4.288	72.321	16.624 ± 0.971	19.153	0.909 ± 0.005	8.233 ± 0.039	8.526
Nb_2AlC	83.370 ± 8.862	82.655	10.220 ± 1.086	12.002	0.575 ± 0.007	5.302 ± 0.005	5.343
TiNbAlC	Ti: 25.828 ± 1.650 Nb: 53.827 ± 5.522	Ti: 26.627 Nb: 51.682	12.826 ± 1.316	15.009	0.578 ± 0.040	6.174 ± 0.273	6.681
TiCrAlC	-	Ti: 34.473 Cr: 37.446	-	19.431	0.900 ± 0.032	8.988 ± 0.213	8.650
TiVAlC	Ti: 35.278 ± 2438 V: 37.880 ± 2618	Ti: 34.736 V: 36.968	17.719 ± 1224	19.580	0.718 ± 0.007	8.839 ± 0.129	8.716
CrVAlC	Cr: 50.712 ± 3216 V: 22.154 ± 1.405	Cr: 36.635 V: 35.892	18.757 ± 1.190	19.011	1.355 ± 0.064	7.710 ± 0.447	8.462
NbVAlC	Nb: 52.877 ± 4.690 V: 26.552 ± 2.355	Nb: 50.813 V: 27.861	12.730 ± 1.129	14.757	0.699 ± 0.014	6.501 ± 0.246	6.569
NbCrAlC	-	Nb: 50.521 Cr: 28.275	-	14.672	0.431 ± 0.006	5.189 ± 0.193	6.531

Table 8
Mechanical properties gathered from hardness and indentation tests.

	Hardness HV_{30}	Indentation Hardness HM (300mN) [N/mm^2]	Indentation Modulus (300mN) [GPa]	Indentation Hardness HM (30mN) [N/mm^2]	Indentation Modulus (30mN) [GPa]
Ti_2AlC	649 ± 26	7114 ± 340	171.44 ± 5.27	10843 ± 3756	197.60 ± 38.79
Cr_2AlC	544 ± 41	6569 ± 702	201.63 ± 8.21	8680 ± 673	212.98 ± 11.44
V_2AlC	408 ± 106	6629 ± 534	179.16 ± 13.83	8050 ± 706	195.92 ± 10.10
Nb_2AlC	795 ± 51	7567 ± 1230	192.51 ± 9.75	10043 ± 1146	204.835 ± 16.67
TiNbAlC	807 ± 58	8791 ± 454	204.41 ± 4.08	9618 ± 940	201.30 ± 13.03
TiCrAlC	1186 ± 42	11548 ± 898	214.38 ± 3.70	13497 ± 1367	223.65 ± 13.95
TiVAlC	564 ± 11	7037 ± 655	206.14 ± 6.88	10199 ± 913	224.79 ± 10.95
CrVAlC	696 ± 36	7164 ± 567	209.56 ± 11.64	10004 ± 560	219.71 ± 7.07
NbVAlC	898 ± 31	8937 ± 878	208.32 ± 12.63	11044 ± 2209	239.62 ± 32.51
NbCrAlC	1185 ± 35	13402 ± 4930	224.09 ± 12.02	14138 ± 1562	243.23 ± 16.38

compounds have smaller lattice parameters calculated from X-Ray diffraction (Table 6). These observations lead to conclusion, that within small oxygen content (up to 1 % wt.), the differences between the mechanical properties are more likely to be the result of the residual porosity and inherent properties of the material, determined by type of atoms (and bond strength) within the MAX phase crystal structure. In the case of Ti-Cr-Al-C and Nb-Cr-Al-C bulks, higher hardness and elastic moduli are the result of the MX carbide and MA intermetallic structure (Fig. 3).

3.4. Thermal oxidation of powders

The mass loss of the samples during the initial stage of the heating (up to 200 °C), particularly visible during heating of Cr_2AlC (Fig. 4a) and CrVAlC (Fig. 4b), can be attributed to evaporation of water adsorbed by the powder material [59]. While most of the MAX phases gained between 3–5 % of mass due to oxidation, Ti_2AlC reached the value of 7.73 % (Fig. 4a). It has been previously reported that increased oxygen content within the MAX phase lattice decreases the onset temperature of MAX phase oxidation [60], which may signify the partial substitution of carbon atoms by oxygen when its content reaches a certain level, which is visible only for Ti_2AlC that had the highest oxygen content (2.1 %) of synthesized powders (Table 7). Another possible factor promoting the oxidation of Ti_2AlC is larger content of secondary phases – Ti_3AlC_2 and Al_2O_3 (Tables 3 and 4), particularly Ti_3AlC_2, which is also known to have inferior oxidation resistance in comparison with Ti_2AlC [61] due to

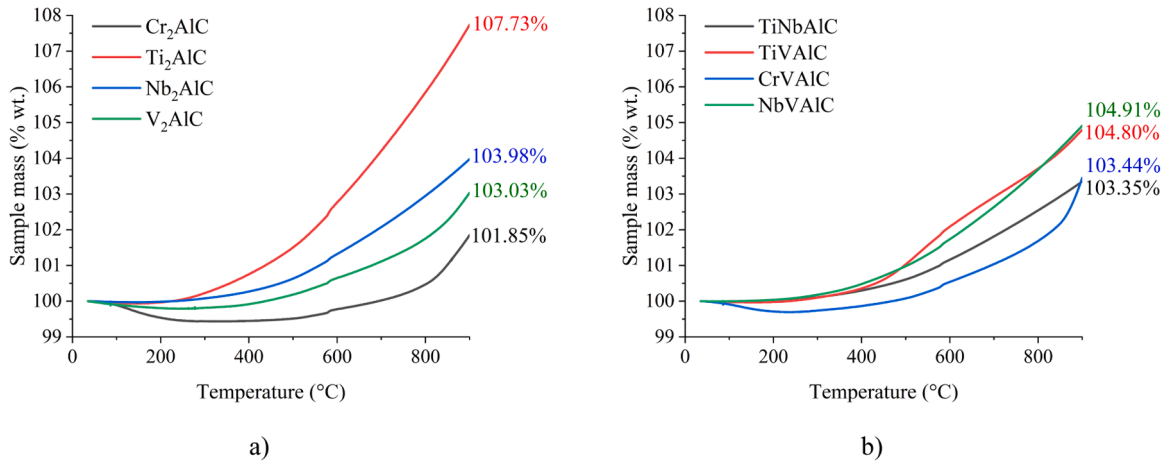

Fig. 4. Thermogravimetric curves: MAX phase powders (a) and MMAX phase powders (b).

the higher concentration of aluminum, increasing the possibility of alumina layer formation, preventing further oxidation [62]. Improvement on the phase purity as well as limitation of oxygen contamination of Ti_2AlC by using the methods mentioned in paragraph 3.1. could improve the oxidation resistance of this MAX phase.

4. Conclusions

The synthesis of MAX phases still poses a significant challenge, where precise optimization of the precursor stoichiometries and high-temperature synthesis parameters of the powder mixture is required to achieve optimal purity. The HEBM-PSPS synthesis route resulted in formation of relatively pure quaternary MAX phases, apart from TiCrAlC and NbCrAlC, due to limitations of the components solubility. The microstructure observations confirmed the presence of residual porosity after low-temperature FAST/SPS densification, as well as presence of residual MX carbides and MA intermetallics. The EDS microanalysis also confirmed the presence of aluminum oxide, that is present in all synthesized MAX phases. The chemical composition assessment indicates that the synthesized MAX phases are slightly aluminum-deficient. The elastic modulus of synthesized MAX and MMAX phases was slightly lower than those typically reported, due to the remaining porosity after FAST/SPS densification. The highest values of hardness and elastic modulus were obtained from the niobium-containing ternary (Nb_2AlC) and quaternary (TiNbAlC and NbVAlC) MAX phases. The high oxygen content of Ti_2AlC resulted in increased oxidation rate during TG tests. Further study will be made on their functional properties as dense bulks and coatings, such as tribological wear and corrosion resistance as well as oxidation performance.

CRediT authorship contribution statement

Tsipas Sophia Alexandra: Writing – review & editing, Supervision, Methodology, Conceptualization. **Kania Albert:** Methodology, Investigation. **Kubicki Grzegorz:** Writing – review & editing, Writing – original draft, Methodology, Investigation, Funding acquisition, Formal analysis, Data curation, Conceptualization. **Wiśniewski Jakub:** Writing – review & editing, Writing – original draft, Visualization, Investigation, Data curation. **Jakubowicz Jarosław:** Writing – review & editing, Supervision. **Garbiec Dariusz:** Writing – review & editing, Supervision, Project administration, Funding acquisition. **Patalas Adam:** Investigation.

Funding

The research work was carried out as part of Applied Doctorate programme funded by Ministry of Education and Science (currently Ministry of Science and Higher Education) Project Agreement No. DWD/5/0214/2021.

This work was supported by the European Union through the Horizon Europe programme under GA number 101135965.

Declaration of Competing Interest

The authors declare that they have no known competing financial interests or personal relationships that could have appeared to influence the work reported in this paper.

Appendix A. Supporting information

Supplementary data associated with this article can be found in the online version at doi:10.1016/j.jallcom.2025.180272.

References

[1] H. Rohde, H. Kudielka, Strukturuntersuchungen an Carbosulfiden von Titan und Zirkon 114 (1960) 447–456.
[2] W. Jeitschko, H. Nowotny, F. Benesovsky, Kohlenstoffhaltige ternäre Verbindungen (H-Phase), Monatshefte für Chemie und verwandte Teile anderer Wissenschaften 94 (1963) 672–676.
[3] Z. Li, Z. Wang, G. Ma, R. Chen, W. Yang, K. Wang, P. Ke, A. Wang, High-performance Cr2AlC MAX phase coatings for ATF application: Interface design and oxidation mechanism, Corros. Commun. 13 (2024) 27–36.
[4] M.W. Barsoum, T. El-Raghy, Synthesis and characterization of a remarkable ceramic: Ti3SiC2, J. Am. Ceram. Soc. 79 (1996) 1953–1956.
[5] M. Naguib, V.N. Mochalin, M.W. Barsoum, Y. Gogotsi, 25th Anniversary Article: MXenes: a new family of two-dimensional materials, Adv. Mater. 26 (2014) 992–1005.
[6] M.S. Alam, M.A. Chowdhury, M.A. Kowser, M.S. Islam, M.M. Islam, T. Khandaker, Advances of MAX phases: synthesis, characterizations and challenges, Eng. Rep. 6 (2024) e12911.
[7] M. Guo, G. Cao, H. Pan, J. Guo, C. Chen, B. Zhang, J. Hu, Recent progress in synthesis of MAX phases and oxidation & corrosion mechanism: a review, Mater. Res. Lett. 12 (2024) 765–796.
[8] C. Ma, W. Yu, Y. Ma, G. Ma, H. Wang, Atomic level out-diffusion and interfacial reactions of MAX phases in contact with metals and air, J. Eur. Ceram. Soc. 44 (2024) 1–22.
[9] A. Shamsipoor, B. Mousavi, M. Razavi, M. Bahamirian, M. Farvizi, Cr2AlC MAX phase: a promising bond coat TBC material with high resistance to high temperature oxidation, Ceram. Int. 51 (2025) 6439–6447.
[10] X. Fan, S. Li, W. Zhang, X. Zhang, J. Mou, Low infrared emissivity of a Ti3AlC2 MAX ceramic for high-temperature thermal camouflage, J. Eur. Ceram. Soc. 44 (2024) 5503–5515.
[11] M.S. Alam, M.A. Chowdhury, T. Khandaker, M.S. Hossain, M.S. Islam, M.M. Islam, M.K. Hasan, Advancements in MAX phase materials: structure, properties, and novel applications, RSC Adv. 14 (2024) 26995–27041.
[12] M. Dahlqvist, M.W. Barsoum, J. Rosen, MAX phases – past, present, and future, Mater. Today 72 (2024) 1–24.
[13] H. Xiao, S. Zhao, J. Zhang, S. Zhao, Y. Li, K. Chen, L. Cao, Y. Wang, Q. Huang, C. Wang, Distinct amorphization resistance in high-entropy MAX-phases (Ti, M)

2AlC (M=Nb, Ta, V, Zr) under in situ irradiation, npj Comput. Mater. 10 (2024) 196.
[14] M.A.M. Filho, W. Farmer, C.-L. Hsiao, R.B. dos Santos, L. Hultman, J. Birch, K. Ankit, G.K. Gueorguiev, Density functional theory-fed phase field model for semiconductor nanostructures: the case of self-induced core–shell InAlN nanorods, Cryst. Growth Des. 24 (2024) 4717–4727.
[15] K. Ma, X. Shi, G. He, J. Li, J. Xu, J. Zuo, M. Li, In situ reaction synthesis, microstructure and thermomechanical properties of novel medium-entropy (Ti,V, Nb,Ta)2AlC ceramics, Ceram. Int. 49 (2023) 21206–21212.
[16] H. Zou, W. Zhang, J. Zhang, L. Ren, W. Wang, F. Zhang, Z. Fu, Synthesis of a novel textured high entropy M4AlC3 (M = Ti, V, Mo, Nb, Ta) composites with improved mechanical properties via spark plasma sintering, J. Eur. Ceram. Soc. 44 (2024) 6889–6900.
[17] Z. Wu, X. Zhu, Y. Shen, X. Zong, Y. Wu, Q. Wang, J. Tang, Z. Wang, H. Zhu, X. Yuan, Z. Zhou, X. Liu, X. Zhang, H. Wang, S. Jiang, M.J. Kim, Z. Lu, High-entropy MAX phase with ultrahigh strength and large plasticity mediated by local chemical fluctuations, Mater. Today (2024).
[18] W. Luo, X. Jiang, Y. Liu, X. Yuan, J. Huo, P. Li, S. Guo, Entropy-driven morphology regulation of MAX phase solid solutions with enhanced microwave absorption and thermal insulation performance, Small 20 (2024) 2305453.
[19] L. Qiao, J. Bi, G. Liang, Y. Yang, H. Wang, S. Wang, Synthesis of high-entropy MXenes with high-efficiency electromagnetic wave absorption, J. Adv. Ceram. 12 (2023) 1902–1918.
[20] X. Zhao, Y. Chen, M. Feng, C. Xu, J. Du, X. Wang, Z. Liu, Synthesis, calculations and energy storage applications of high-entropy MXene, J. Alloy. Compd. 992 (2024).
[21] V. Desai, A. Shrivastava, A. Zala, T. Parekh, S. Gupta, N.I. Jamnapara, Pressureless manufacturing of high purity Ti3AlC2 MAX phase material: Synthesis and characterisation, Vacuum 214 (2023) 112221.
[22] A.A. Sijuade, F.L. Bellevu, S.K.Devendhar Singh, M.M. Rahman, N. Arnett, O. I. Okoli, Processing of V2AlC MAX phase: optimization of sintering temperature and composition, Ceram. Int. 50 (2024) 3733–3738.
[23] S. Haji Amiri, N. Pourmohammadie Vafa, Microstructure and mechanical properties of Ti3SiC2 MAX phases sintered by hot pressing, Synth. Sinter. 1 (2021) 216–222.
[24] A. Dash, Y.J. Sohn, R. Vaßen, O. Guillon, J. Gonzalez-Julian, Synthesis of Ti3SiC2 MAX phase powder by a molten salt shielded synthesis (MS3) method in air, J. Eur. Ceram. Soc. 39 (2019) 3651–3659.
[25] A. Tsyganov, M. Vikulova, A. Shindrov, D. Zheleznov, A. Gorokhovsky, N. Gorshkov, Molten salt-shielded synthesis of Ti3AlC2 as a precursor for large-scale preparation of Ti3C2Tx MXene binder-free film electrode supercapacitors, Dalton Trans. 53 (2024) 5922–5931.
[26] K. Sobolev, A. Pazniak, O. Shylenko, V. Komanicky, A. Provino, P. Manfrinetti, D. Peddis, V. Rodionova, Complex optimization of arc melting synthesis for bulk Cr2AlC MAX-phase, Ceram. Int. 47 (2021) 7745–7752.
[27] N. Laska, P.-P. Bauer, O. Helle, F. Kreps, Sputtering and characterization of MAX-phase forming Cr–Al–C and Ti–Al–C coatings and their application on γ-based titanium aluminides, Adv. Eng. Mater. 24 (2022) 2100722.
[28] Y. Xu, Y. Zhang, A. Zhang, G. Ma, Z. Wang, A. Wang, HiPIMS induced a facile synthesis of Ti3SiC2 MAX phase coating at 850 °C, Surf. Coat. Technol. 501 (2025) 131930.
[29] A. Hendaoui, D. Vrel, A. Amara, A. Benaldjia, P. Langlois, Ti-Al-C MAX phases by aluminothermic reduction process, Int. J. Self-propagating High. -Temp. Synth. 17 (2008) 125–128.
[30] S. Aydinyan, Combustion synthesis of MAX phases: microstructure and properties inherited from the processing pathway, Crystals (2023).
[31] K.D. Verma, K.K. Kar, Cost-effective synthesis route for ultra-high purity of Ti3AlC2 MAX phase with enhanced performance of Ti3C2Tx MXene and MXene/NiO composite for supercapacitor application, Chem. Eng. J. 504 (2025) 158938.
[32] M. Yunus, R. Kumar, B. Maji, M. Krishnan, An optimized method for synthesizing phase-pure Ti3AlC2 MAX-phase through spark plasma sintering, J. Eur. Ceram. Soc. 42 (2021).
[33] S.N. Perevislov, I.E. Arlashkin, V.L. Stolyarova, Synthesis and sintering of MAX phases in the Zr–Al–C system, J. Am. Ceram. Soc. 107 (2024) 488–500.
[34] M. Ge, X. Wang, G. Li, C. Lu, J. Zhang, R. Tu, Synthesis of Cr2AlC from elemental powders with modified pressureless spark plasma sintering, J. Wuhan. Univ. Technol. -Mater. Sci. Ed. 34 (2019) 287–292.
[35] R. Yamanoglu, Pressureless spark plasma sintering: a perspective from conventional sintering to accelerated sintering without pressure, Powder Metall. Met. Ceram. 57 (2019) 513–525.
[36] E. Tabares, S.C. Cifuentes, A. Jiménez-Morales, S.A. Tsipas, Injection moulding of porous MAX phase Ti3SiC2 without using space-holder, Powder Technol. 380 (2021) 96–105.
[37] E. Tabares, A. Jiménez-Morales, S.A. Tsipas, Study of the synthesis of MAX phase Ti3SiC2 powders by pressureless sintering, Boletín de la Sociedad Española de Cerámica y Vidrio 60 (2021) 41–52.
[38] J. Wozniak, A. Jastrzębska, A. Olszyna, Challenges and opportunities in tailoring MAX phases as a starting materials for MXenes development, Mater. Technol. 37 (2022) 1639–1650.
[39] I. Roslyk, I. Baginskiy, V. Zahorodna, O. Gogotsi, S. Ippolito, Y. Gogotsi, Porous Ti3AlC2 MAX phase enables efficient synthesis of Ti3C2T MXene, Int. J. Appl. Ceram. Technol. 21 (2024) 2605–2612.
[40] Z. Zhang, S.H. Lim, J. Chai, D.M.Y. Lai, A.K.H. Cheong, K.L. Cheong, S.J. Wang, H. Jin, J.S. Pan, Plasma spray of Ti2AlC MAX phase powders: effects of process parameters on coatings' properties, Surf. Coat. Technol. 325 (2017) 429–436.
[41] Z. Zhang, S.H. Lim, J. Chai, D.M.Y. Lai, P.C. Lim, A.K.H. Cheong, S. Wang, H. Jin, J. Pan, Kerosene-fuelled high velocity oxy-fuel (HVOF) spray of Ti2AlC MAX phase powders, J. Alloy. Compd. 735 (2018) 377–385.
[42] W. Zhang, S. Li, X. Zhang, X. Chen, Research and development on cold-sprayed MAX phase coatings, : Coat. (2023).
[43] N. Shahin, A. Heidarpour, S. Kazemi, Synthesis of Ti3SiC2 MAX Phases by High Energy Ball Milling of Elemental Powders of Ti, Si and graphite C (2016).
[44] N. Shahin, S. Kazemi, A. Heidarpour, Mechanochemical synthesis mechanism of Ti3AlC2 MAX phase from elemental powders of Ti, Al and C, Adv. Powder Technol. 27 (2016) 1775–1780.
[45] H. Rietveld, A profile refinement method for nuclear and magnetic structures, J. Appl. Crystallogr. 2 (1969) 65–71.
[46] W.C. Oliver, G.M. Pharr, An improved technique for determining hardness and elastic modulus using load and displacement sensing indentation experiments, J. Mater. Res. 7 (1992) 1564–1583.
[47] W.C. Oliver, G.M. Pharr, Measurement of hardness and elastic modulus by instrumented indentation: advances in understanding and refinements to methodology, J. Mater. Res. 19 (2004) 3–20.
[48] Z.G. Liu, L.L. Ye, J.T. Guo, G.S. Li, Z.Q. Hu, Self-propagating high-temperature synthesis of TiC and NbC by mechanical alloying, J. Mater. Res. 10 (1995) 3129–3135.
[49] N. Shahin, A. Heidarpour, S. Kazemi, The purity evolution of TiAlC MAX phase synthesized by mechanochemical route: the effect of Al content and high-temperature annealing, Eng. Rep. 6 (2024) e12814.
[50] L. Hemati, M. Farvizi, S.A. Ataie, L. Nikzad, E. Ghasali, A. Faraji, T. Liskiewicz, Microstructure and mechanical properties of (CrxTi1-x)2AlC 211 MAX phases as composites through spark plasma sintering, Ceram. Int. 50 (2024) 27806–27822.
[51] J.C. Schuster, H. Nowotny, C. Vaccaro, The ternary systems: CrAlC, VAlC, and TiAlC and the behavior of H-phases (M2AlC), J. Solid State Chem. 32 (1980) 213–219.
[52] B. Mansouri, M. Rafiei, I. Ebrahimzadeh, F. Naeimi, M. Barekat, The effect of milling time and heat treatment on the synthesis of the Cr2AlC MAX phase, Can. Metall. Q. 63 (2024) 970–980.
[53] J. Halim, P. Chartier, T. Basyuk, T. Prikhna, E.A.N. Caspi, M.W. Barsoum, T. Cabioc'h, Structure and thermal expansion of (Crx,V1−x)n+ 1AlCn phases measured by X-ray diffraction, J. Eur. Ceram. Soc. 37 (2017) 15–21.
[54] M.W. Barsoum, I. Salama, T. El-Raghy, J. Golczewski, H.J. Seifert, F. Aldinger, W. D. Porter, H. Wang, Thermal and electrical properties of Nb2AlC, (Ti, Nb)2AlC and Ti2AlC, Metall. Mater. Trans. A 33 (2002) 2775–2779.
[55] B. Scheibe, V. Kupka, B. Peplińska, M. Jarek, K. Tadyszak, The influence of oxygen concentration during MAX phases (Ti3AlC2) preparation on the α-Al2O3 microparticles content and specific surface area of multilayered MXenes (Ti3C2Tx), Materials 12 (2019) 353.
[56] P.P. Michałowski, M. Anayee, T.S. Mathis, S. Kozdra, A. Wójcik, K. Hantanasirisakul, I. Jóźwik, A. Piątkowska, M. Możdżonek, A. Malinowska, R. Diduszko, E. Wierzbicka, Y. Gogotsi, Oxycarbide MXenes and MAX phases identification using monoatomic layer-by-layer analysis with ultralow-energy secondary-ion mass spectrometry, Nat. Nanotechnol. 17 (2022) 1192–1197.
[57] J. Wang, Y. Zhou, T. Liao, J. Zhang, Z. Lin, A first-principles investigation of the phase stability of Ti2AlC with Al vacancies, Scr. Mater. 58 (2008) 227–230.
[58] M.W. Barsoum, The M+ 1 AX phases and their properties, Ceram. Sci. Technol. (2010) 299–347.
[59] T.S. Mathis, K. Maleski, A. Goad, A. Sarycheva, M. Anayee, A.C. Foucher, K. Hantanasirisakul, C.E. Shuck, E.A. Stach, Y. Gogotsi, Modified MAX phase synthesis for environmentally stable and highly conductive Ti3C2 MXene, ACS Nano 15 (2021) 6420–6429.
[60] M. Anayee, M. Shekhirev, R. Wang, Y. Gogotsi, Effect of oxygen substitution and oxycarbide formation on oxidation of Ti3AlC2 MAX phase, J. Am. Ceram. Soc. 107 (2024) 6334–6341.
[61] X. Li, X. Xie, J. Gonzalez-Julian, R. Yang, R. Schwaiger, J. Malzbender, Oxidation and creep behavior of textured Ti2AlC and Ti3AlC2, J. Eur. Ceram. Soc. 42 (2022) 364–375.
[62] D.J. Tallman, A. Babak, M.W. Barsoum, A critical review of the oxidation of Ti2AlC, Ti3AlC2 and Cr2AlC in air, Mater. Res. Lett. 1 (2013) 115–125.